www.ietdl.org

Published in IET Power Electronics
Received on 16th January 2014
Revised on 18th March 2014
Accepted on 29th April 2014
doi: 10.1049/iet-pel.2014.0044

ISSN 1755-4535

Finite control set predictive control based on Lyapunov function for three-phase voltage source inverters

Sangshin Kwak, Sung-Jin Yoo, Juncheol Park

School of Electrical and Electronics Engineering, Chung-Ang University, Seoul, Korea
E-mail: sskwak@cau.ac.kr

Abstract: A Lyapunov-function-based technique for finite control set predictive control is proposed to control the load currents of three-phase voltage source inverters (VSIs). The developed technique, based on a discrete-time model of a VSI, determines a control law using the Lyapunov function. Based on the Lyapunov stability analysis considering inevitable quantisation errors between the proposed control law and control actions selected from the inherent finite control set of the VSI, all signals of the closed-loop dynamics are uniformly ultimately bounded and the current control errors converge to a neighbourhood of the origin. In addition to rendering the finite control set predictive control system globally stable, the proposed Lyapunov-function-based finite control set predictive control reduces the amount of calculations required to predict a future variable by half compared with the conventional finite control set predictive control, resulting in lower actuation time delay. Experimental results with three-phase VSIs are presented to validate the proposed Lyapunov-function-based control method.

1 Introduction

Feedback-based output current control of three-phase voltage source inverters (VSIs) has been considered one of the most important areas of research in past decades. Proportional–integral control methods with distinct pulsewidth modulation (PWM) blocks and non-linear hysteresis current controls have been widely employed for current control of VSIs [1, 2]. Besides the traditional current control schemes, finite control set predictive control (FCS-PC), based on inherent finite control actions because of switching operation, has been recently developed as a simple and effective control method for power converters. Owing to its simplicity with no individual PWM blocks as well as its control flexibility, the FCS-PC methods have been utilised to control different properties of diverse power converter structures. The FCS-PC scheme has been employed to control the output currents of a variety of power converters, such as three-phase VSIs, multilevel inverters, multiphase inverters, active power filters and matrix converters [3–12, 19, 20]. Moreover, by using the FCS-PC technique to predict the future behaviours of power and torque as well as current, it has been applied for direct torque control and direct power control of motor drives and active front-end rectifiers [7, 11]. The FCS-PC algorithm predicts possible future behaviours of converters based on the system model as well as present values, and then judges all the predicted values by the predefined cost function for a given time horizon. Owing to this operating scheme, one of the concerns of the FCS-PC method may be heavy computational load, which can lead to a considerable time delay in the controller, which in turn can deteriorate system performance [13]. As a result, it is desirable to develop a control method that carries out fewer calculations. Furthermore, a complete research on the three-phase VSI, considering practical issues and experiments, with explicit address of the stability issues of the FCS-PC method are, in terms of the entire power converter systems, lacking in the areas of power electronics.

In this paper, a Lyapunov-function-based control strategy based on an FCS model is proposed to control the load currents of three-phase VSI. Since the proposed controller is designed based on the Lyapunov stability theorem, the developed FCS-PC can explicitly provide a globally stable control law. In the Lyapunov stability analysis, inevitable quantisation errors between the proposed control law and the finite number of control actions generated by inherent switching operations of the VSI are also considered. It is proved that all signals of the closed-loop dynamics are uniformly ultimately bounded and the current control errors converge to a neighbourhood of the origin. Furthermore, the proposed control strategy calculates an affirmative future voltage reference vector by using the system model, which can produce the future load current closest to the future current reference. Owing to the unique voltage reference vector, the amount of calculations for the proposed Lyapunov-function-based FCS-PC method to predict a future variable is reduced by half compared with the conventional FCS-PC. Total execution time of the proposed FCS-PC algorithm is reduced by about 80% of that of the conventional FCS-PC method, since the proposed method is subject to half amount of calculation amount to predict

future variables compared with the conventional method. Comprehensive investigations of the proposed algorithm are presented to show effects of estimation errors of back-electromotive force (back-emf), future reference current vectors and total harmonic distortions. Experimental results are included to support the feasibility of the proposed Lyapunov-function-based FCS-PC.

2 Conventional FCS predictive current control

The FCS-PC method originated from the fact that power converters can generate only a finite number of switching states, providing a finite number of control inputs to loads. For the three-phase VSI shown in Fig. 1, six active and two zero vectors can be produced to adjust output quantities such as load currents [3, 4, 18]. Since the two zero vectors generate equal output voltages, only seven control sets can be obtained by the three-phase VSI.

The load current dynamics of the three-phase VSI with a three-phase resistive–inductive-active load is expressed in vector form in the $\alpha\beta$ frame as

$$\boldsymbol{v} = R\boldsymbol{i} + L\frac{\mathrm{d}\boldsymbol{i}}{\mathrm{d}t} + \boldsymbol{e} \tag{1}$$

where R, L and $\boldsymbol{e}$ denote load resistance, inductance and back-emf vector, respectively. In addition, $\boldsymbol{v}$ and $\boldsymbol{i}$ imply the voltage vector generated by the VSI and the load current vector, respectively. The derivative of the load current in continuous-time model can be approximated based on the backward finite-difference method, with a sampling period T_s, as

$$\frac{\mathrm{d}\boldsymbol{i}}{\mathrm{d}t} \simeq \frac{\boldsymbol{i}(k) - \boldsymbol{i}(k-1)}{T_s} \tag{2}$$

Using (2), the load current dynamics of (1) in the continuous-time domain can be replaced in discrete-time domain as

$$\boldsymbol{i}(k+1) = \frac{1}{RT_s + L}\left[L\boldsymbol{i}(k) + T_s\boldsymbol{v}(k+1) - T_s\boldsymbol{e}(k+1)\right] \tag{3}$$

The conventional FCS-PC method is based on the property that the seven consequent future current values produced by the seven voltage vectors of the VSI can be predicted based on the load model of (3). Using this property, each predicted future current value in the $\alpha\beta$ frame is evaluated by the predefined cost function to select the optimal switching state at the next step as

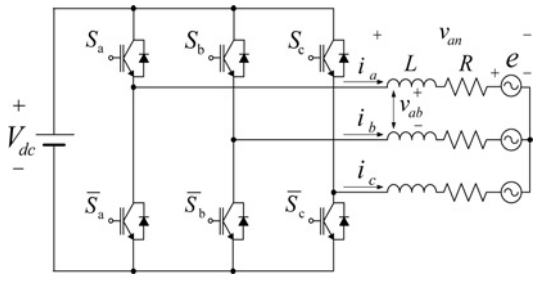

Fig. 1 *Three-phase VSI with RLe load*

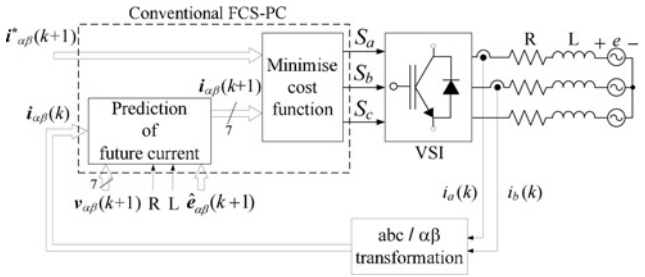

Fig. 2 *Block diagram of conventional FCS-PC method*

$$\begin{aligned} g = &\left|i^*_\alpha(k+1) - i_\alpha(k+1)\right| \\ &+ \left|i^*_\beta(k+1) - i_\beta(k+1)\right| \end{aligned} \tag{4}$$

where $i^*_\alpha(k+1)$ and $i^*_\beta(k+1)$ are the future current values. The optimal future switching state selected from the cost function can force the future load current value to approach the reference load current value at the next step. Finally, the selected voltage state at the next sampling instant, which can minimise the current error, is applied to the load by the VSI. Fig. 2 illustrates the block diagram of the conventional FCS-PC approach for control of the load current of the three-phase VSI. As can be seen in Fig. 2, each block of the FCS-PC requires seven repeated calculations to obtain the possible future current values and to judge all the possible future current values. Moreover, the conventional FCS-PC only depends on currents, and relates no reference voltage with current errors. Therefore the stability issues cannot be explicitly addressed in the conventional FCS-PC, which does not have any control laws obtained from a systematic analytical design approach. Accordingly, the FCS-PC approach is proposed based on the Lyapunov stability theorem [14–16].

3 Proposed Lyapunov-function-based FCS-PC

In this section, the FCS-PC method, based on Lyapunov stability analysis, is established to control the load currents of the VSI and describe related issues in terms of the entire VSI system with RLe loads. For comprehensive stability analysis with practical voltage choice in the finite set, seven fixed voltage vectors allowed by the VSI, which serve as control inputs, are considered as

$$\begin{aligned} \boldsymbol{v}(k+1) \in U := \Big\{ &0,\ \frac{2}{3}V_{\mathrm{dc}}\mathrm{e}^{\mathrm{j}0},\ \frac{2}{3}V_{\mathrm{dc}}\mathrm{e}^{\mathrm{j}(\pi/3)},\ \frac{2}{3}V_{\mathrm{dc}}\mathrm{e}^{\mathrm{j}(2\pi/3)}, \\ &\frac{2}{3}V_{\mathrm{dc}}\mathrm{e}^{\mathrm{j}\pi},\ \frac{2}{3}V_{\mathrm{dc}}\mathrm{e}^{\mathrm{j}(4\pi/3)},\ \frac{2}{3}V_{\mathrm{dc}}\mathrm{e}^{\mathrm{j}(5\pi/3)} \Big\} \end{aligned} \tag{5}$$

The voltage vector constrained in the finite set is, then, expressed with the continuous voltage and the quantisation error vectors as

$$\boldsymbol{v}(k+1) = \bar{\boldsymbol{v}}(k+1) + \boldsymbol{\delta}(k+1) \tag{6}$$

where $\bar{\boldsymbol{v}}(k+1)$ is the continuous voltage input vector and $\boldsymbol{\delta}(k+1)$ is the quantisation error vector. The future current control

error in the discrete-time domain is defined as

$$\tilde{\boldsymbol{i}}(k+1)=\boldsymbol{i}(k+1)-\boldsymbol{i}^{*}(k+1)$$
$$=\frac{1}{RT_{\mathrm{s}}+L}\left[L\boldsymbol{i}(k)+T_{\mathrm{s}}\boldsymbol{v}(k+1)-T_{\mathrm{s}}\boldsymbol{e}(k+1)\right]-\boldsymbol{i}^{*}(k+1) \tag{7}$$

where $\boldsymbol{i}^{*}(k+1)$ is the future reference load current vector.

Lemma 1: The solutions of the dynamics (3) are practically exponentially stable if there exists an input $v \in U$ such that $\tilde{i} \in G$ and if there exists a continuous function $V[\tilde{\boldsymbol{i}}(k)]$ satisfying the following inequality

$$\begin{aligned} &V\left[\tilde{\boldsymbol{i}}(k)\right] \geq c_1\left|\tilde{\boldsymbol{i}}(k)\right|^{l}, \quad \forall \tilde{\boldsymbol{i}}(k) \in G \\ &V\left[\tilde{\boldsymbol{i}}(k)\right] \leq c_2\left|\tilde{\boldsymbol{i}}(k)\right|^{l}, \quad \forall \tilde{\boldsymbol{i}}(k) \in \Gamma \\ &V\left[\tilde{\boldsymbol{i}}(k+1)\right]-V\left[\tilde{\boldsymbol{i}}(k)\right]<-c_3\left|\tilde{\boldsymbol{i}}(k)\right|^{l}+c_4 \end{aligned} \tag{8}$$

where c_1, c_2, c_3 and c_4 are positive constants, $l \geq 1$, $G \subseteq \mathbb{R}^n$ is a control positive invariant set and $\Gamma \subseteq G$ is a compact set.

Theorem 1: Consider the load current dynamics controlled by the following Lyapunov-function-based FCS-PC law

$$\bar{v}(k+1)=-\frac{L}{T_{\mathrm{s}}}i(k)+\frac{RT_{\mathrm{s}}+L}{T_{\mathrm{s}}}i^{*}(k+1)+\hat{e}(k) \tag{9}$$

where $\hat{\boldsymbol{e}}(k)$ is an estimated back-emf vector. Then, the closed-loop system (3) with control law (9) is practically exponentially stable in the following compact set

$$\Lambda=\left\{\tilde{i}\middle|\left\|\tilde{i}\right\| \leq \left(\frac{T_{\mathrm{s}}}{RT_{\mathrm{s}}+L}\right)(\phi+\varepsilon)\right\} \tag{10}$$

where a constant ϕ and ε are the upper bound of the quantisation error vector and the estimation error of back-emf vector, respectively.

Proof: Define the discrete Lyapunov function, which is definitely positive, as

$$V\left[\tilde{\boldsymbol{i}}(k)\right]=\frac{1}{2}\tilde{\boldsymbol{i}}^{\mathrm{T}}(k)\tilde{\boldsymbol{i}}(k) \tag{11}$$

Using (7), the rate of change of the Lyapunov function is expressed as (see (12))

Assume that the estimation error of back-emf vector is bounded by a constant value $\varepsilon \geq \|\boldsymbol{e}(k+1)-\hat{\boldsymbol{e}}(k)\|$. Since the voltage vector $\boldsymbol{v}(k+1)$ is constrained in the finite set, the load current $\boldsymbol{i}(k)$ is bounded, and thus the current control error is bounded, that is, $\tilde{\boldsymbol{i}}(k) \in \Gamma \subset R^2$ where Γ is a compact set determined by the finite set of the voltage vector and the bounded reference load current vector. In addition, $\bar{\boldsymbol{v}}(k+1)$ is bounded because of the boundedness of $\boldsymbol{i}(k)$, $\boldsymbol{i}^{*}(k+1)$ and $\hat{\boldsymbol{e}}(k)$ in (9). Thus, for all $\tilde{\boldsymbol{i}}(k) \in \Gamma$, there exists a constant $\phi>0$ satisfying $\left\|\boldsymbol{\delta}(k+1)\right\| \leq \phi$. By applying the control law (9), the rate of change of the Lyapunov function can be

$$\Delta V(k) \leq -\frac{1}{2}\tilde{\boldsymbol{i}}^{\mathrm{T}}(k)\tilde{\boldsymbol{i}}(k)+\frac{1}{2}\left(\frac{T_{\mathrm{s}}}{RT_{\mathrm{s}}+L}\right)^{2}(\phi+\varepsilon)^{2} \tag{13}$$

Therefore the condition (8) is satisfied by defining

$$\begin{aligned} c_1 &= c_2 = 1 \\ c_3 &= \frac{1}{2} \\ c_4 &= \frac{1}{2}\left(\frac{T_{\mathrm{s}}}{RT_{\mathrm{s}}+L}\right)^{2}(\phi+\varepsilon)^{2} \end{aligned} \tag{14}$$

Therefore the closed-loop system is practically exponentially stable. The inequality (13) can be rewritten as

$$\Delta V(k) \leq -2c_3 V\left[\tilde{\boldsymbol{i}}(k)\right]+c_4 \tag{15}$$

This inequality implies that, as time increases, the current control errors converge in the compact set as

$$\Lambda=\left\{\tilde{i}\middle|\left\|\tilde{i}\right\| \leq \sqrt{c_4/c_3}\right\} \tag{16}$$

Remark 1 (estimations of future reference and future back-emf vectors): Based on (9), the future output voltage vector can be obtained by measuring the present load current $\boldsymbol{i}(k)$ as well as by estimating the future reference current and the back-emf vectors. The future value of the reference current vector can be obtained from the Lagrange extrapolation formula by [4, 17]

$$\boldsymbol{i}^{*}(k+1) \simeq \hat{\boldsymbol{i}}^{*}(k+1)=3\boldsymbol{i}^{*}(k)-3\boldsymbol{i}^{*}(k-1)+\boldsymbol{i}^{*}(k-2) \tag{17}$$

For a sufficiently small sampling period, the future reference current vector can be assumed to be equal to the present reference current vector as $\boldsymbol{i}^{*}(k+1) \simeq \boldsymbol{i}^{*}(k)$. Similarly, the future back-emf vector can be estimated by a second-order extrapolation or can be assumed to be equal to the present back-emf vector as $\boldsymbol{e}(k+1) \simeq \boldsymbol{e}(k)$. The present back-emf vector can be calculated by shifting (11) backward in time, as

$$\boldsymbol{e}(k+1) \simeq \hat{\boldsymbol{e}}(k)=\boldsymbol{v}(k)+\frac{L}{T_{\mathrm{s}}}\boldsymbol{i}(k-1)-\frac{RT_{\mathrm{s}}+L}{T_{\mathrm{s}}}\boldsymbol{i}(k) \tag{18}$$

In the proposed approach, the control law in (9) is used as the future reference voltage vector $\bar{\boldsymbol{v}}^{*}(k+1)$, in order to choose one of seven future voltage vectors of the VSI in a finite set. If the future voltage vector of the VSI closest to the future reference voltage vector obtained from (9) is applied to the VSI, the load current at the next sampling instant tracks the future reference current. Since the VSI only generates the seven voltage vectors in its finite set in

$$\Delta V(k)=V\left[\tilde{\boldsymbol{i}}(k+1)\right]-V\left[\tilde{\boldsymbol{i}}(k)\right]=\frac{1}{2}\left(\frac{1}{RT_{\mathrm{s}}+L}\left\{L\boldsymbol{i}(k)+T_{\mathrm{s}}\bar{\boldsymbol{v}}(k+1)+T_{\mathrm{s}}\boldsymbol{\delta}(k+1)-T_{\mathrm{s}}\left[\boldsymbol{e}(k+1)-\hat{\boldsymbol{e}}(\boldsymbol{k})\right]\right\}-\boldsymbol{i}^{*}(k+1)\right)^{\mathrm{T}}$$
$$\times\left(\frac{1}{RT_{\mathrm{s}}+L}\left\{L\boldsymbol{i}(k)+T_{\mathrm{s}}\bar{\boldsymbol{v}}(k+1)+T_{\mathrm{s}}\boldsymbol{\delta}(k+1)-T_{\mathrm{s}}\left[\boldsymbol{e}(k+1)-\hat{\boldsymbol{e}}(\boldsymbol{k})\right]\right\}-\boldsymbol{i}^{*}(k+1)\right)-\frac{1}{2}\tilde{\boldsymbol{i}}^{\mathrm{T}}(k)\tilde{\boldsymbol{i}}(k) \tag{12}$$

doi: 10.1049/iet-pel.2014.0044

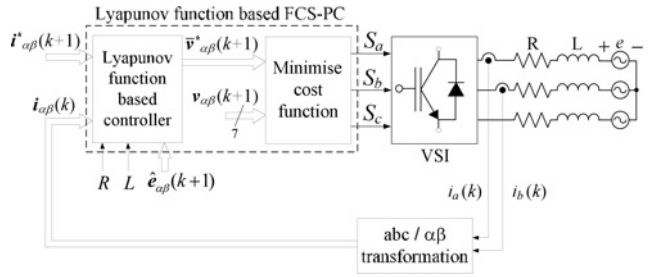

Fig. 3 *Block diagram of proposed Lyapunov-function-based FCS-PC method*

contrast to the continuous reference voltage vector in (9), the cost function defined as (19) enables one proper future voltage vector to be selected among seven possible vectors

$$g = \left|v^*_\alpha(k+1) - v_\alpha(k+1)\right| + \left|v^*_\beta(k+1) - v_\beta(k+1)\right| \tag{19}$$

Note that the quantisation error caused by (19) is also considered in the stability analysis of Theorem 1. Fig. 3 shows the block diagram of the proposed Lyapunov-function-based FCS-PC. As clearly shown in Fig. 3, the Lyapunov-function-based controller generates the single confirmative control law $\vec{v}^*(k+1)$, using the measured load current as well as the estimated back-emf and the future reference current vector in addition to the load resistor and inductor (RL) parameters. Consequently, the controller block requires only one calculation to predict the future reference voltage vector, while predicting the future reference current vector in the conventional FCS-PC method needs seven repetitive calculations as shown in Fig. 2. Thus, the proposed control method can reduce the total amount of calculation, in comparison with the conventional FCS-PC.

Remark 2 (effects of back-emf estimation error): Since the back-emf vector in practical applications varies with much slower frequency, generally a few tens Hz, compared with the sampling period, the future back-emf vector is estimated in (18). Therefore the error between the real future back-emf vector $\boldsymbol{e}(k+1)$ and the estimated back-emf vector $\hat{\boldsymbol{e}}(k)$ consists of the one-step delay error and the calculation error of the present back-emf vector constructed with available voltage vector and current vector in (18). By assuming sinusoidal back-emf voltages, the two error components of the back-emf estimation, normalised by the peak value of the back-emf vector, are defined by

$$\text{one-step delay error(\%)} = \frac{(1/T_\text{f})\int_0^{T_\text{f}} \left|\boldsymbol{e}(k+1) - \boldsymbol{e}(k)\right| \text{d}t}{\text{peak value of } \boldsymbol{e}(k)} \times 100(\%) \tag{20}$$

$$\text{calculation error(\%)} = \frac{(1/T_\text{f})\int_0^{T_\text{f}} \left|\boldsymbol{e}(k) - \hat{\boldsymbol{e}}(k)\right| \text{d}t}{\text{peak value of } \boldsymbol{e}(k)} \times 100(\%) \tag{21}$$

where T_f is the fundamental frequency of the back-emf vector. The one-step delay error in the back-emf estimation as functions of the sampling period and the back-emf frequency is shown in Fig. 4. It can be seen that the error increases proportional to the sampling period, because larger sampling period results in increased delay error. Moreover, the faster fundamental frequency of the back-emf voltage increases the error resulted from one-step delay, because of increased rate of changes during one-step size.
The calculation error in the back-emf estimation as functions of the sampling period and the back-emf frequency is also shown in Fig. 5. Contrary to the one-step delay error, the calculation error increases in inversely proportion to the sampling period. In addition, faster fundamental frequency of the back-emf voltage increases the calculation error. Overall, the total error of the back-emf vector estimation is shown in Fig. 6.

Remark 3 (effects of future reference current vector estimation error): The one-step future reference current vector is estimated from the Lagrange extrapolation formula using the present and the two past reference current vectors in (17), based on the fact that the sampling period is constant. An error between the real and the estimated future reference current vectors based on the quadratic prediction values, normalised by the magnitude of the future reference

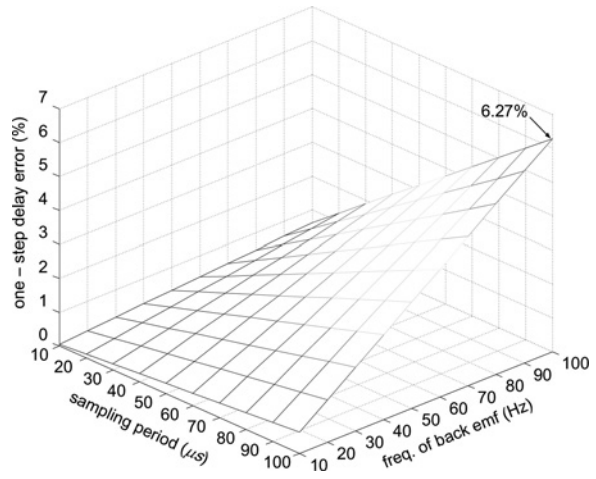

Fig. 4 *One-step delay error in back-emf estimation as functions of sampling period and back-emf frequency (V_{dc} = 100 V, R = 1 Ω and L = 8 mH)*

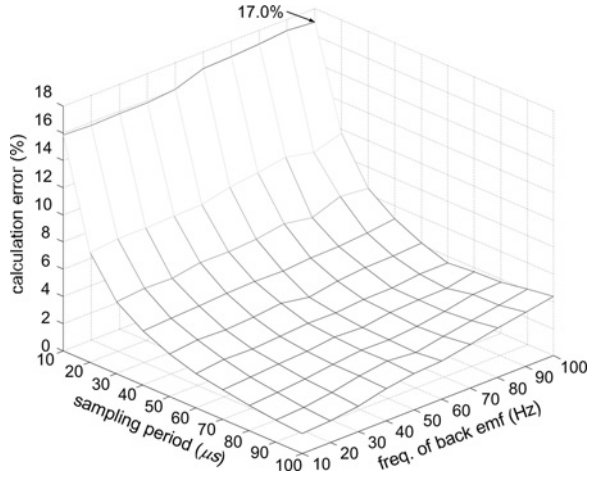

Fig. 5 *Calculation error in back-emf estimation as functions of sampling period and back-emf frequency (V_{dc} = 100 V, R = 1 Ω and L = 8 mH)*

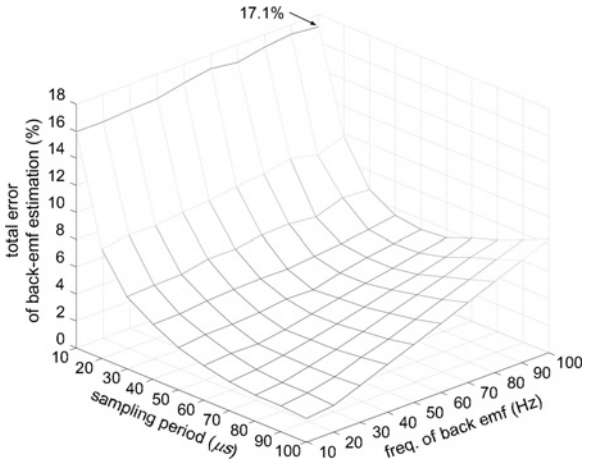

Fig. 6 *Total error of back-emf vector estimation as functions of sampling period and back-emf frequency (V_{dc} = 100 V, R = 1 Ω and L = 8 mH)*

current vector, is defined as

$$\text{error of future reference current estimation (\%)} = \frac{(1/T_{\text{f}})\int_0^{T_{\text{f}}} \left|\boldsymbol{i}^*(k+1) - \hat{\boldsymbol{i}}^*(k+1)\right| \mathrm{d}t}{\text{peak value of } \boldsymbol{i}^*(k)} \times 100(\%) \quad (22)$$

where T_{f} implies the frequency of the reference current vector. Fig. 7 illustrates the errors of the future reference current estimation against the sampling period and the reference current frequency. As can be seen from Fig. 7, the errors increase proportional to the sampling period and the reference current frequency. It is obvious that the errors resulted from the Lagrange extrapolation formula are negligible, which is <0.02%, in the case of 100 μs sampling period and 100 Hz reference current.

4 Experimental results

The proposed FCS-PC method based on Lyapunov function was tested with a prototype setup. The setup consisted of a three-phase VSI with an insulated gate bipolar transistor (IGBT) module and a dc-link capacitor with V_{dc} = 100 V

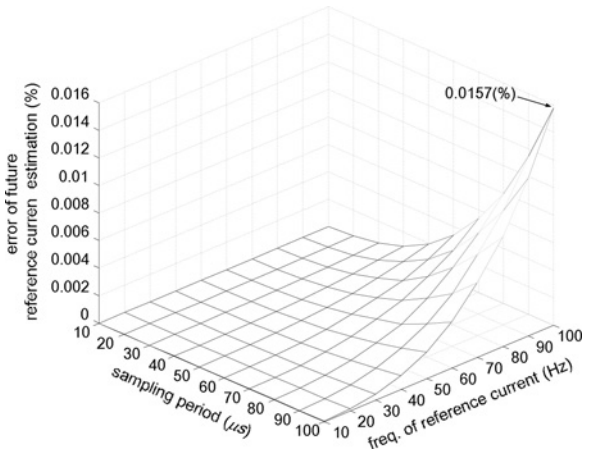

Fig. 7 *Errors of future reference current estimation against sampling period and reference current frequency*

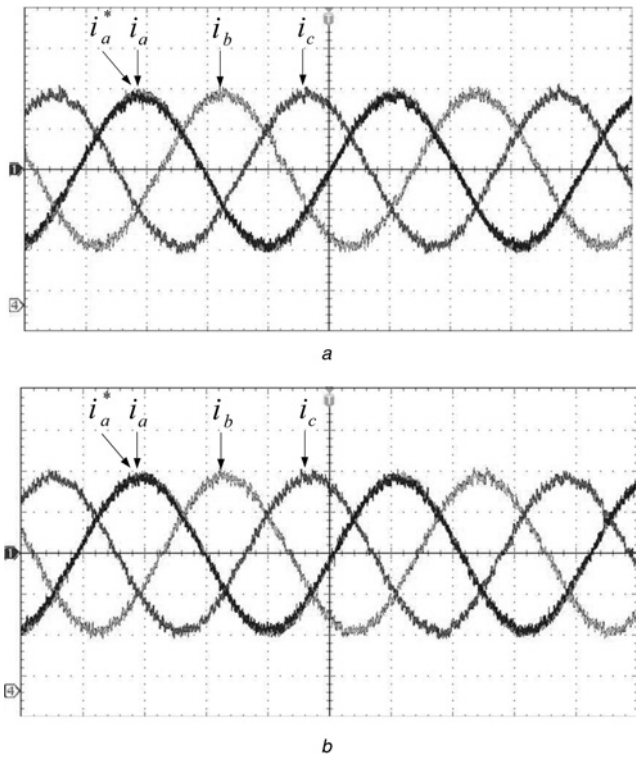

Fig. 8 *Three-phase output currents (i_a, i_b and i_c) (2 A/div and 4 ms/div) and a-phase reference current (i_a^*) (2 A/div and 4 ms/div) for T_s = 50 μs obtained*

a From the conventional FCS-PC
b From the proposed Lyapunov-function-based FCS-PC

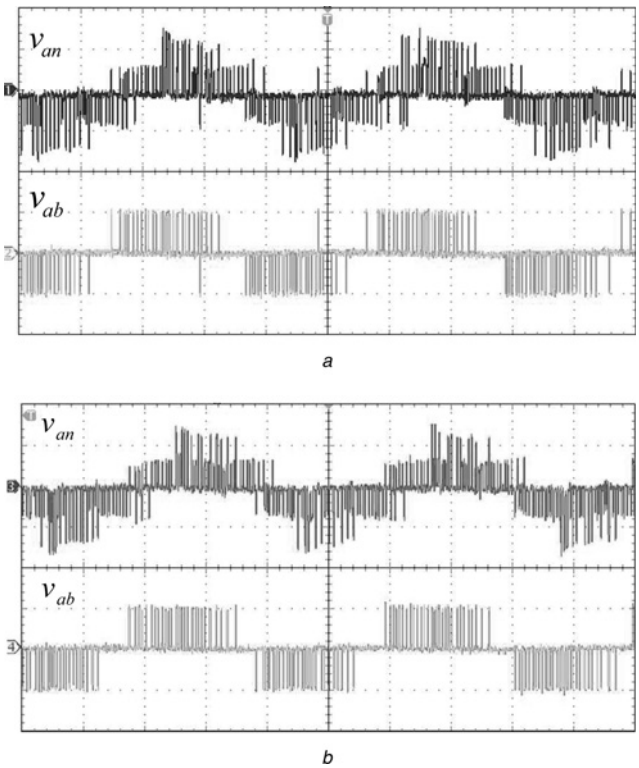

Fig. 9 *Output phase voltage (50 V/div and 4 ms/div) and line-to-line voltage (100 V/div and 4 ms/div) for T_s = 50 μs obtained*

a From the conventional FCS-PC
b From the proposed Lyapunov-function-based FCS-PC

doi: 10.1049/iet-pel.2014.0044

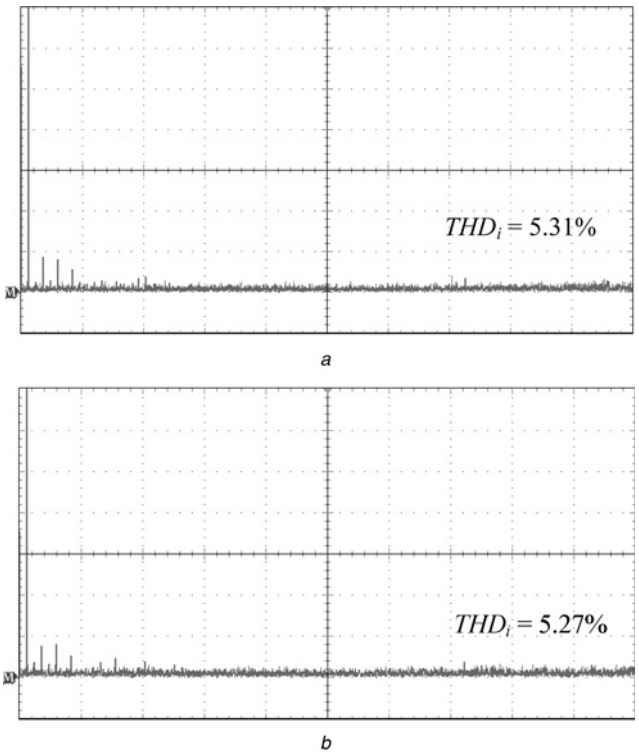

Fig. 10 *Frequency spectrum of output current (i_a) ($T_s = 50$ μs) from*

a Conventional FCS-PC (20 mV/div and 500 Hz/div)
b Proposed Lyapunov-function-based FCS-PC (20 mV/div and 500 Hz/div)

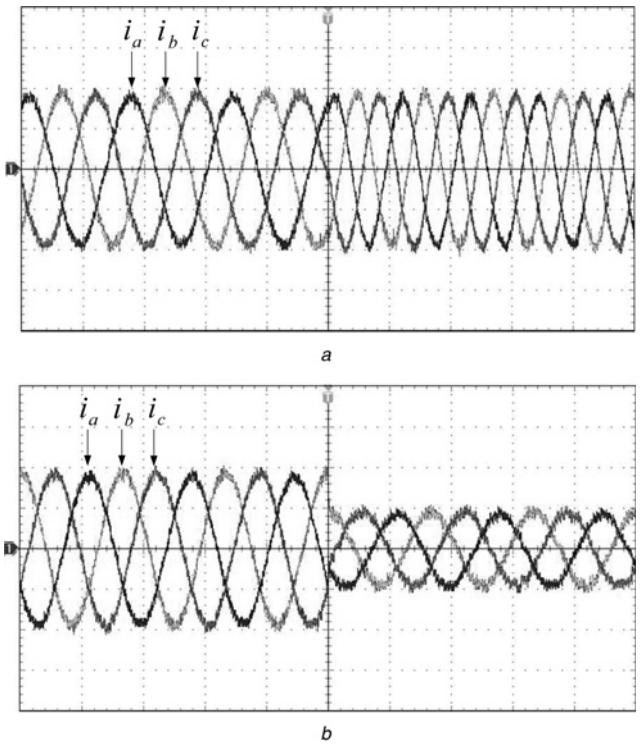

Fig. 11 *Three-phase output currents (i_a, i_b and i_c) obtained from the proposed Lyapunov-function-based FCS-PC for $T_s = 50$ μs (2 A/div and 10 ms/div)*

a Under frequency step change from 60 to 90 Hz
b Under magnitude step change

and a Texas Instrument digital signal processor (DSP) board (TMS320F28335) with an RL load ($R = 1$ Ω and $L = 6$ mH). Fig. 8 illustrates the experimental results of the *a*-phase reference current and the three-phase actual output currents obtained from the conventional and the proposed FCS-PC methods for the RL load. It is seen that the real output currents controlled by the proposed control method accurately track the reference current, like those controlled by the conventional FCS-PC method. The output line-to-line voltage and the phase voltage generated by the conventional and the proposed FCS-PC methods are shown in Fig. 9. The frequency spectrums of the load currents obtained from the conventional and the proposed FCS-PC methods for $T_s = 50$ μs are compared in Fig. 10. The harmonic analysis in this paper considered was set to consider up to 80th harmonic components with inter-harmonic components ignored, in calculating the total harmonic distortion (THD) values. It is observed that the two control methods result in almost the same THDs of the load currents.

In the experimental setup, the execution time required to complete the whole algorithms of the conventional FCS-PC and the proposed Lyapunov-function-based FCS-PC methods were calculated by measuring calculation cycles of the DSP board. Total execution time of the proposed scheme corresponds to about 80% total execution time of the conventional FCS-PC algorithm, which is illustrated in Table 1. Therefore it is experimentally proved that the proposed Lyapunov-function-based FCS-PC method exhibits the same output performances as well as reduced execution time, in comparison with the conventional FCS-PC scheme.

Table 1 Measurement of execution times

	Conventional FCS-PC	Proposed Lyapunov-function-based FCS-PC	Comparison, %
Execution time, μs	8.34	6.87	−18

The dynamic responses for the sampling time $T_s = 50$ μs are shown in Fig. 11. It is obviously seen that the three-phase load currents controlled by the proposed control scheme follow the reference change with fast dynamics, under both step changes.

The discrete Lyapunov functions obtained by experimental results are shown in Fig. 12 under transient conditions. The figure shows that the discrete Lyapunov function, which corresponds to the square load current error, is bounded because of its stability under transient conditions with

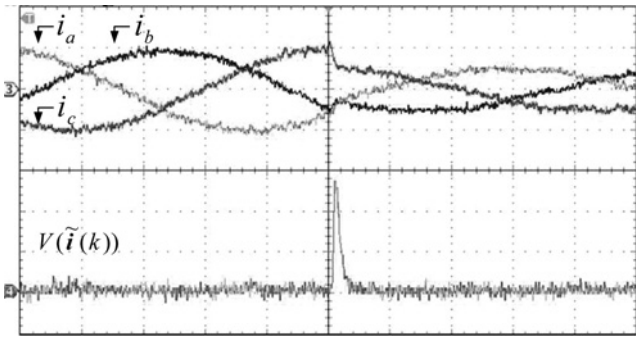

Fig. 12 *Experimental waveforms of VSI output currents (4 A/div and 2 ms/div) and Lyapunov function V(k) (1.33 A^2/div and 2 ms/div) under step change of output current references ($T_s = 50$ μs)*

quantisation errors resulted from the finite number of voltage vectors of the VSI.

5 Conclusion

A Lyapunov-function-based FCS-PC was proposed to control the load currents of the three-phase VSI. In the proposed control scheme, a control law was generated based on the system model and the present load current, in which the derivative of the Lyapunov function is always kept negative. Although maintaining the same performance and dynamics as the conventional FCS-PC, the proposed approach can render a systematic and analytic design methodology that guarantees globally stability as well as reduced amount of calculations by 20% compared with the conventional FCS-PC method. Comprehensive investigations of the proposed algorithm are presented to show effects of estimation errors of back-emf and future reference current vectors and model errors, in addition to total harmonic distortions. Experimental results with three-phase VSIs are presented to validate the proposed Lyapunov-function-based control method with comparative results with the conventional method.

6 Acknowledgment

This work was supported by the National Research Foundation of Korea (NRF) grant funded by the Korea government (MSIP) (2014R1A2A2A01006684).

7 References

1 Kazmierkowski, M.P., Krishnan, R., Blaabjerg, F.: 'Control in power electronics' (Academic, New York, 2002)
2 Mohan, N., Underland, T.M., Robbins, W.P.: 'Power electronics' (Wiley, New York, 2nd edn.)
3 Kouro, S., Cortes, P., Vargas, R., Ammann, U., Rodriguez, J.: 'Model predictive control – a simple and powerful method to control power converters', *IEEE Trans. Ind. Electron.*, 2009, **56**, (6), pp. 1826–1838
4 Rodríguez, J., Pontt, J., Silva, C., Correa, P., Lezana, P., Cortés, P., Ammann, U.: 'Predictive current control of a voltage source inverter', *IEEE Trans. Ind. Electron.*, 2007, **54**, (1), pp. 495–503
5 Lezana, P., Aguilera, R., Quevedo, D.E.: 'Model predictive control of an asymmetric flying capacitor converter', *IEEE Trans. Ind. Electron.*, 2009, **56**, (6), pp. 1839–1846
6 Vargas, R., Cortes, P., Ammann, U., Rodriguez, J., Pontt, J.: 'Predictive control of a three-phase neutral-point-clamped inverter', *IEEE Trans. Ind. Electron.*, 2007, **54**, (5), pp. 2697–2705
7 Cortes, P., Rodriguez, J., Antoniewicz, P., Kazmierkowski, M.: 'Direct power control of an AFE using predictive control', *IEEE Trans. Power Electron.*, 2008, **23**, (5), pp. 2516–2523
8 Correa, P., Rodriguez, J., Rivera, M., Espinoza, J.R., Kolar, J.W.: 'Predictive control of an indirect matrix converter', *IEEE Trans. Ind. Electron.*, 2009, **56**, (6), pp. 1847–1853
9 Muller, S., Ammann, U., Rees, S.: 'New time-discrete modulation scheme for matrix converters', *IEEE Trans. Ind. Electron.*, 2005, **52**, (6), pp. 1607–1615
10 Vargas, R., Ammann, U., Rodriguez, J., Pontt, J.: 'Predictive strategy to control common-mode voltage in loads fed by matrix converters', *IEEE Trans. Ind. Electron.*, 2008, **55**, (12), pp. 4372–4380
11 Vargas, R., Ammann, U., Hudoffsky, B., Rodriguez, J., Wheeler, P.: 'Predictive torque control of an induction machine fed by a matrix converter with reactive input power control', *IEEE Trans. Power Electron.*, 2010, **25**, (6), pp. 1426–1438
12 Cortes, P., Rodriguez, J., Quevedo, D.E., Silva, C.: 'Predictive current control strategy with imposed load current spectrum', *IEEE Trans. Power Electron.*, 2008, **23**, (2), pp. 612–618
13 Cortes, P., Rodriguez, J., Silva, C., Flores, A.: 'Delay compensation in model predictive current control of a three-phase inverter', *IEEE Trans. Ind. Electron.*, 2012, **59**, (2), pp. 1323–1325
14 Khalil, H.K.: 'Nonlinear systems' (Prentice-Hall, Upper Saddle River, NJ, 2001)
15 Meza, C., Biel, D., Jeltsema, D., Scherpen, J.: 'Lyapunov-based control scheme for single-phase grid-connected PV central inverters', *IEEE Trans. Control Syst. Technol.*, 2012, **20**, (2), pp. 520–528
16 Rahmani, S., Hamdi, A., Al-Haddad, K.: 'A Laypunov-function-based control for three-phase shunt hybrid active filter', *IEEE Trans. Ind. Electron.*, 2012, **59**, (3), pp. 1418–1429
17 Kukrer, O.: 'Discrete-time current control of voltage-fed three-phase PWM inverters', *IEEE Trans. Ind. Electron.*, 1996, **11**, (2), pp. 260–269
18 Park, G., Lee, S., Jin, S., Kwak, S.: 'Integrated modeling and analysis of dynamics for electric vehicle powertrains', *Expert Syst. Appl.*, 2014, **41**, (5), pp. 2595–2607
19 Han, Y., Xu, L.: 'Design and implementation of a robust predictive control scheme for active power filters', *J. Power Electron.*, 2011, **11**, (5), pp. 751–758
20 Atia, Y., Salem, M.: 'Microcontroller-based improved predictive current controlled VSI for single-phase grid-connected systems', *J. Power Electron.*, 2013, **13**, (6), pp. 1016–1023

doi: 10.1049/iet-pel.2014.0044